



MOX-Report No. 95/2021

Prediction of myocardial blood flow under stress conditions by means of a computational model

Di Gregorio, S.; Vergara, C.; Montino Pelagi, G.; Baggiano, A.;
Zunino, P.; Guglielmo, M.; Fusini, L.; Muscogiuri, G.; Rossi,
A.; Rabbat, M.G.; Quarteroni, A.; Pontone, G.

MOX, Dipartimento di Matematica
Politecnico di Milano, Via Bonardi 9 - 20133 Milano (Italy)

mox-dmat@polimi.it

<http://mox.polimi.it>

Prediction of myocardial blood flow under stress conditions by means of a computational model

Simone Di Gregorio^{a,*}, PhD, Christian Vergara^{b,*}, PhD, Giovanni Montino Pelagi^a, MSc, Andrea Baggiano^{c,d}, MD, Paolo Zunino^a, PhD, Marco Guglielmo^c, MD, Laura Fusini^c, MD, Giuseppe Muscogiuri^c, MD, Alexia Rossi^{e,f}, MD, Mark G. Rabbat^{g,h}, MD, Alfio Quarteroni^{a,i}, Prof, Gianluca Pontone^c, MD, PhD

* These authors equally contributed to the work

^a MOX, Dipartimento di Matematica, Politecnico di Milano, Milan, Italy

^b LABS, Dipartimento di Chimica, Materiali e Ingegneria Chimica, Politecnico di Milano, Milan, Italy

^c Cardiovascular Imaging Department, Centro Cardiologico Monzino IRCSS, Milan, Italy

^d Department of Clinical Science and Community Health, University of Milan, Milan, Italy

^e Department of Nuclear Medicine, University Hospital, Zurich, Switzerland

^f Center for Molecular Cardiology, University of Zurich, Zurich, Switzerland

^g Loyola University of Chicago, Chicago, IL, United States of America

^h Edward Hines Jr. VA Hospital, Hines, IL, United States of America

ⁱ Institute of Mathematics, Ecole Polytechnique Fédérale de Lausanne, Switzerland
(professor emeritus)

Address for correspondence: Gianluca Pontone

Via C. Parea 4, 20138, Milano, Italy

Phone: +39 02 58002574; +39 347 1217311,

Fax: +39 02 58002231

Email: gianluca.pontone@ccfm.it

ORCID

Simone Di Gregorio: 0000-0001-5875-5359

Christian Vergara: 0000-0001-9872-5410

Andrea Baggiano: 0000-0002-8261-4529

Paolo Zunino: 0000-0002-2470-0189

Marco Guglielmo: 0000-0003-1718-9949

Laura Fusini: 0000-0003-0309-6231

Giuseppe Muscogiuri: 0000-0003-4757-2420

Alexia Rossi: 0000-0001-6845-1199

Mark G. Rabbat: 0000-0002-1936-0079

Alfio Quarteroni: 0000-0002-5947-6885

Gianluca Pontone: 0000-0002-1339-6679

ABSTRACT

Purpose. Quantification of myocardial blood flow (MBF) and functional assessment of coronary artery disease (CAD) can be achieved through stress myocardial computed tomography perfusion (stress-CTP). This requires an additional scan after the resting coronary computed tomography angiography (cCTA) and administration of an intravenous stressor. This complex protocol has limited reproducibility and non-negligible side effects for the patient. We aim to mitigate these drawbacks by proposing a computational model able to reproduce MBF maps.

Methods. A computational perfusion model was used to reproduce MBF maps. The model parameters were estimated by using information from cCTA and MBF measured from stress-CTP (MBF_{CTP}) maps. The relative error between the computational MBF under stress conditions (MBF_{COMP}) and MBF_{CTP} was evaluated to assess the accuracy of the proposed computational model.

Results. Applying our method to 9 patients (4 control subjects without ischemia vs 5 patients with myocardial ischemia), we found an excellent agreement between the values of MBF_{COMP} and MBF_{CTP} . In all patients, the relative error was below 8% over all the myocardium, with an average-in-space value below 4%.

Conclusion. The results of this pilot work demonstrate the accuracy and reliability of the proposed computational model in reproducing MBF under stress conditions. This consistency test is a preliminary step in the framework of a more ambitious project which is currently under investigation, i.e. the construction of a computational tool able to predict MBF avoiding the stress protocol and potential side effects while reducing radiation exposure.

KEY WORDS: Cardiac perfusion, computed tomography, coronary artery disease, myocardial blood flow, computational model

INTRODUCTION

The detection of coronary artery stenosis and associated ischemia is of utmost importance in the identification of patients who should be addressed for further invasive evaluation and revascularization. To this regard, the combined use of coronary computed tomography angiography at rest (cCTA) and stress myocardial computed tomography perfusion (stress-CTP) have been recently introduced to obtain both anatomical and functional analysis of coronary artery disease (CAD) with one imaging test [1-4]. cCTA ensures CAD detection from an anatomical point of view, whereas stress-CTP allows the evaluation of myocardial perfusion through the measurement of myocardial blood flow (MBF) under pharmacologically induced stress conditions [5,6]. The drawback is that stress-CTP requires an additional scan on top of cCTA and an intravenous stressor administration with an increase of radiation exposure and potential stressor related side effects.

Computational models have shown to be an effective tool in cardiovascular clinical practice. The best-known example in the CAD clinical setting is HeartFlow[®], which, starting from anatomical information about epicardial coronary arteries obtained from cCTA, computes fractional flow reserve (FFR) non-invasively, by means of computational fluid dynamics (CFD) simulations. Over the past few years, computational models were also used to study myocardial perfusion for a better understanding of myocardial ischaemia [7-12]. However, only recently have computational tools been applied to real data for a quantitative analysis of cardiac perfusion, representing a challenging task to achieve [12].

In this study we provide a first assessment of the reliability of computational tools in reproducing MBF maps. In particular, our starting point is the previous work by Di Gregorio et al [9] where we proposed a new computational framework for the computation of blood flow maps. This model is based on the mathematical coupling between the fluid-dynamics in the large coronary (those detectable by the standard CT images), where 3D Navier-Stokes equations are considered, and that in the small coronaries and microcirculation, addressed by means of a homogenization assumption that leads to the equations of a fluid in a porous medium (multi-compartment Darcy equations). Our hypothesis was that the computational model developed in [9], complemented by patient specific data, could predict MBF maps under stress conditions. The aim of this work is to present a methodology to calibrate in a patient-specific setting the parameters of the computational model and to compare the results of the computational estimates of MBF of 9 patients with the stress-CTP based measures.

MATERIALS AND METHODS

Fig. 1 demonstrates a pipeline overview of the methods.

Study Population and acquisition of clinical data

The dataset was related to patients with a clinical indication for invasive coronary angiography with FFR assessment evaluated with a coronary CT angiography (cCTA) at rest plus myocardial CTP scan under stress extracted from the cohort of PERFECTION trial [4-6]. We randomly extracted 4 patients without ischemia (P1 to P4) and 5 patients with ischemia (P5 to P9) with functionally significant CAD as detected by invasive coronary angiography with FFR assessment (Table 1).

Rest cCTA was performed with a Revolution CT scanner (GE Healthcare, Milwaukee, Wisconsin). The following parameters were used: slice configuration 256x0.625 mm, spatial resolution 0.23 mm; gantry rotation time 280 ms; tube voltage was 120kV for patient P8 (BMI of 30 kg/m²), while other patients were assessed with 100 kV; effective tube current ranged between 500 mA and 600 mA according to patient BMI (500 mA if BMI < 25 kg/m², 550 mA if 25 < BMI < 30 kg/m², 600 mA if BMI ≥ 30 kg/m²).

Stress-CTP scans were performed after vasodilatation induced with an intravenous adenosine injection (0.14 mg/kg/min over 4 min). At the end of the third minute of adenosine injection the stress-CTP acquisition was performed during free breathing.

To quantify the MBF from stress-CTP (MBF_{CTP}), the arterial input function was sampled in the ascending aorta and the myocardial time-attenuation curves were coupled with arterial input function using a deconvolution model obtained by an adiabatic approximation to the 'tissue homogeneity model', a simplified version of Johnson and Wilson model. MBF_{CTP} was obtained by tissue residue function (i.e. the mass of contrast in tissue over time) [13]. The study protocol was approved by the institutional ethics committee.

Patient-specific geometric reconstruction

Three-dimensional geometries of epicardial coronary arteries and the left ventricle myocardium were reconstructed from the resting cCTA. We performed a semi-automatic segmentation and generated a volumetric computational mesh, composed by hexahedral elements (Fig. 2(A-B)). The open-source software MITK (<http://www.mitk.org/wiki/MITK>) and VMTK [14], together with novel meshing tools [15] were used. Epicardial coronary arteries were reconstructed until the diameter of 1 mm according to the resolution of the cCTA. Below this value it was hard to clearly detect the vessel, so that the reconstruction would be not accurate. To describe the perfusion for smaller vessels, we considered a

homogenization process so that the domain of interest is the whole left ventricle myocardium. In particular, from each outlet of an epicardial coronary artery, the myocardial territory perfused by that specific outlet was identified following the strategy described in Di Gregorio et al [9]. We obtained as many perfusion regions from epicardial coronary artery outlets we could reconstruct from cCTA (Fig. 2(C)).

Computational model

The computational model used to compute patient-specific MBF maps is built on a multi-physics framework based on the following models.⁹

- Blood flow in the reconstructed epicardial coronary arteries was described by the 3D incompressible Newtonian Navier-Stokes (NS) equations (Fig. 2);
- Blood flow in the intramural vessels was modeled as a three-compartment porous medium (multicompartment Darcy (MD) model), where fluid mass balance equations were considered in the whole myocardium domain:

$$\begin{aligned}
 \mathbf{u}_{M,1} + \mathbf{K}_1 \nabla p_{M,1} &= \mathbf{0} \\
 \nabla \cdot \mathbf{u}_{M,1} &= \sum_{j=1}^J \frac{\chi_{\Omega_M^j}}{|\Omega_M^j|} \int_{\Gamma^j} \mathbf{u}_C \cdot \mathbf{n} d\gamma - \beta_{1,2}(p_{M,1} - p_{M,2}) \\
 \mathbf{u}_{M,2} + \mathbf{K}_2 \nabla p_{M,2} &= \mathbf{0} \\
 \nabla \cdot \mathbf{u}_{M,2} &= -\beta_{2,1}(p_{M,2} - p_{M,1}) - \beta_{2,3}(p_{M,2} - p_{M,3}) \\
 \mathbf{u}_{M,3} + \mathbf{K}_3 \nabla p_{M,3} &= \mathbf{0} \\
 \nabla \cdot \mathbf{u}_{M,3} &= -\gamma(p_{M,3} - p_{veins}) - \beta_{3,2}(p_{M,3} - p_{M,2})
 \end{aligned}$$

where $\mathbf{u}_{M,x}$ and $p_{M,x}$ are the blood velocity and pressure in compartment $X=1,2,3$; β_{yz} , $y,z=1,2,3$, are the conductances (to be determined) between compartments y and z regulating the pressure drops; \mathbf{K}_i , $i=1,2,3$, are the permeability tensors (to be determined); $p_{veins}=22,5$ mmHg is the given venous pressure; $\gamma=0.0001$ (Pa s)⁻¹ is a drain coefficient; Ω_M^j the myocardial region perfused by the j -th coronary through the interface Γ^j ; χ_A the characteristic function associated to region A .

This model assumes that intramural vessel network (IVN) can be described as a set of interconnected pores inside the cardiac tissue (Fig. 2). This strategy allowed us to account for the different length scales of IVN, ranging from 1 mm (small coronary arteries, compartment 1) to about 10 μ m (capillaries, compartment 3) [16,17];

- NS equations in epicardial coronary arteries and the MD model in the myocardium were coupled by means of suitable mathematical *interface conditions*. The first one is given by the continuity of mass and it is given by the second, fourth, and sixth equations in the multicompartment model. The second one states the continuity of the momentum at the terminal points of epicardial coronary arteries (Fig. 2):

$$p_C - \mu (\nabla \mathbf{u}_C + (\nabla \mathbf{u}_C)^T) \mathbf{n} \cdot \mathbf{n} - \frac{1}{\alpha^j} \int_{\Gamma^j} \mathbf{u}_C \cdot \mathbf{n} d\gamma = \frac{1}{|\Omega_M^j|} \int_{\Omega_M^j} p_{M,1} dx \quad \text{on } \Gamma^j$$

where α^j are the conductances between epicardial coronaries and the myocardium.

At the inlet of each of the two main coronaries (left and right) we assumed a parabolic velocity profile and we prescribed the representative inlet coronary blood flow rate (CBF) reported in Fig. 2(E) [18], whose average-in-time was set in order to match the total amount of flow rate of the patient:

$$\frac{1}{T} \int_0^T CBF(t) dt = MBF_{avg} V_M, \quad (1)$$

where V_M is the myocardial volume perfused by the left and right main coronaries, and MBF_{avg} the average of MBF_{CTP} in the myocardium. For the numerical solution of this coupled problem, we considered the splitting scheme proposed in Di Gregorio et al [9]. Each sub problem has been approximated by means of the Finite Elements (FE) Method used in combination with a semi-implicit backward differentiation formula of order 1 for temporal discretization, with time step $\Delta t = 0.01$ s. We adopted Q1/Q1 FE with SUPG-PSPG [19] stabilization for NS problem, with mesh size $h_{NS} \sim 0.4$ mm, whereas Q1 FE for MD problem solved for the pressure, with mesh size $h_{MD} \sim 1.8$ mm. Such values were seen to provide results which were robust with respect to mesh independency. The computational simulations were performed using life^x (<https://lifex.gitlab.io/lifex>), an in-house software library based on the deal.II FE library [20].

From our computational simulations we obtained blood pressure and flow field in epicardial coronary arteries and in the myocardial perfusion regions. This allowed us to calculate a *computational* MBF (MBF_{COMP}) under stress conditions that is the amount of blood flow that reaches the third (innermost) porous compartment, related to capillaries. The MBF is proportional to the difference of pressures between the second ($p_{M,2}$) and the third ($p_{M,3}$) compartments, through the conductance (inverse of resistance) $\beta_{2,3}$:

$$MBF_{COMP} = \beta_{2,3} (p_{M,2} - p_{M,3}) * 60 \text{ s/min} * 100 \text{ ml.}$$

The dimensional factors 60 s/min and 100 ml were used to express MBF_{COMP} in ml/min/100ml.

Calibration of the model parameters

To reproduce clinical data of MBF maps, the computational simulations required a proper set of physical parameters:

- The conductance α^i regulating the pressure drop between the epicardial and intramural vessels;
- The conductance $\beta_{1,2}$ and $\beta_{2,3}$ regulating the pressure drop between compartments 1 and 2, and 2 and 3, respectively;
- The permeability of K_1 , K_2 , K_3 related to the 3 compartments in the MD problem.

Suitable values of such parameters were estimated for each patient and assumed to vary among the different perfusion regions. This calibration was performed with the following steps (see Fig. 3):

- C1) an estimation exploiting IVN properties and the knowledge of the total flow rate entering in the system;
- C2) an adjustment to account for vasodilation under stress;
- C3) a modification of the parameters at the septum;
- C4) a final adjustment based on MBF_{CTP} .

In C1 we used information from cCTA at rest to determine a first guess for the parameters. In particular, we built a surrogate IVN, generated using the procedure previously described (Fig. 2(D)) [9]. Then, we solved a Poiseuille problem in such a network and we accordingly estimated the conductance as the ratio between the flow rate and the pressure. Notice that the IVN is built only with the purposes of estimating the conductances, the multi-compartment Darcy problem being solved in the whole myocardium domain. As for the permeability, they were initialized based on geometric issues, in particular for each compartment and perfusion region they were given by the ratio between the volume of the vessels involved in the region and the total region volume [9]. In step C2, we accounted for the vasodilation of arteriolar vessels induced by adenosine injection during stress pharmacological conditions. According to studies that highlighted the relationships between microvascular parameters and stress conditions [21], $\beta_{1,2}$, $\beta_{2,3}$, K_1 and K_2 were increased by 10-fold with respect to baseline parameters estimated for resting conditions at C1. A second adjustment was performed at step C3 based on the observation that at the septum the values of $\beta_{1,2}$ and $\beta_{2,3}$ estimated at C2 were lower than the other myocardial regions, leading to a systematic underestimation of MBF_{COMP} with respect to MBF_{CTP} (about 10 times). This may be due to the fact that not all the septal epicardial coronaries could be seen by CT images. To overcome this, we multiplied $\beta_{1,2}$ and $\beta_{2,3}$ at the septum by a factor 5. This

value has been calibrated in order to maximize the accordance with the measured blood flow maps and it seemed to be quite robust with respect to the patient. Finally, in step C4 we started from the values of $\beta_{1,2}$ and $\beta_{2,3}$ obtained at C3 and we corrected them by changing their values to reduce the discrepancies with MBF_{CTP} . If the discrepancy in a perfusion region was such that the computational simulation overestimated the average measured perfusion, then the corresponding $\beta_{1,2}$ and $\beta_{2,3}$ were decreased by a factor proportional to the ratio between MBF_{COMP} and MBF_{CTP} ; otherwise, $\beta_{1,2}$ and $\beta_{2,3}$ were accordingly increased. Notice that the values of $\beta_{1,2}$ and $\beta_{2,3}$ are constant in each perfusion region, with such constants that could be different among different perfusion regions. Instead, we did not consider their variation in time, according to the fact that MBF are steady maps obtained as an average during the diastolic phase.

Errors calculation

For the evaluation of the accuracy of the computational model we calculated the mismatch between measured and computed MBF (error). Given the two perfusion maps under stress conditions, i.e. MBF_{COMP} and MBF_{CTP} , we first defined MBF_{COMP}^i and MBF_{CTP}^i as the corresponding average-in-space values in each j -th perfusion region (Fig. 4). Then, we defined \overline{MBF}_{CTP} as the global perfusion map given by the collection of MBF_{CTP}^i and in an analogous way we introduced the global computed map \overline{MBF}_{COMP} . This allowed us to compute the global error map Err as the collection of the local errors (Fig. 4). Finally, we calculated the mean Err_{mean} of all the errors among the perfusion regions, weighted over the corresponding volume.

To have a clinical evaluation of the myocardial perfusion we also investigated the results exploiting a tetra-colorimetry visualization of \overline{MBF}_{CTP} and \overline{MBF}_{COMP} associated to the entity of myocardial ischemia and CAD. In this way, we were able to recognize the physiological perfused regions (in red - $MBF^i > 150$ ml/min/100ml) from the ischemic ones, and we could evaluate the severity of the myocardial ischemia considering 3 different levels of hypoperfused regions: green - $100 < MBF^i < 150$ ml/min/100ml; light blue - $50 < MBF^i < 100$ ml/min/100ml; blue - $MBF^i < 50$ ml/min/100ml.

RESULTS

The characteristics of the CT scan protocol for both rest and stress acquisitions together with the percentage of perfused volumes were reported in Table 2. Table 3 reports the number of perfusion regions for each patient.

Consistency test

For each patient we reported the values of the discrepancies Err_{mean} (Table 3). The error is always smaller than 4% highlighting a small discrepancy between the computational results and clinical data. In Fig. 5, we showed the comparison between the computational (\overline{MBF}_{COMP}) and the measured (\overline{MBF}_{CTP}) perfusion maps under stress conditions, together with the error Err and the epicardial coronaries and myocardial reconstructions. There was excellent agreement between computational results and clinical data for all patients, as shown by the boxplots of the error Err . We notice that the large errors were obtained for the ischemic patients P6, P7, P8, P9, whose error is also highly variable over the perfusion regions. Probably this was due to the presence of stenotic coronaries that makes the calibration harder. In particular, the relative error was less than 5%, apart from the stenotic cases P6, P8, P9 where not more than 3 regions featured a greater error, less than 7% and with a low variability. These results highlighted the ability of the proposed computational model in reproducing the perfusion maps for both healthy subjects and stenotic patients with great accuracy.

Towards a blind application

Since we aim to predict MBF by means of our computational tool for patients where MBF_{CTP} is not available, it was important to ask the ability of our method to work without this information. MBF_{CTP} was used to suitably calibrate the model parameters (step C4).

In Fig. 6 we reported the computed MBF_{COMP} , together with the error, for three healthy subjects (P2,P3,P4) and one patient with functionally significant CAD (P8) when we used only steps C1-C3. As expected, the errors were increased with respect to the previous analysis. We also reported the tetra-colorimetric maps. Healthy subjects (P2-P4) showed a fully red map (perfusion always greater than the physiological threshold), which was completely predicted by our computations. For P8, there were significant differences.

DISCUSSION

In this work, we report a first analysis on the reliability of a computational model in predicting MBF maps under stress conditions and in providing an alternative to the stress protocol. In particular, we have applied the computational tool proposed in Di Gregorio et al [9] to 9 patients, 4 without and 5 with functionally significant CAD. To the best of our knowledge, this is the first application of a mathematical perfusion model to a real-world data-set with the aim of reproducing MBF.

Our calibration of model parameters was composed by 4 steps, C1-C4. The ultimate goal of this research is to calibrate the computational tool in order to be able to predict MBF with only steps C1-C3. Indeed, these steps are independent of the stress-CTP acquisition: step C1 is obtained by using geometric cCTA data at rest. Steps C2 and C3 are adjusted based on considerations about the vasodilation effect of adenosine and the low MBF_{COMP} at the septum. The only information coming from stress-CTP that has been used in steps C1-C3 is the inlet CBF prescribed at the inlet of the epicardial coronaries. However, inlet CBF, i.e. the amount of blood flow incoming in the most proximal coronaries (see Figure 2) could be alternatively measured by other techniques, such as Doppler ultrasound. Thus, steps C1-C3 could lead to a calibration which is completely CTP free, leading to a computational tool which may be an alternative to stress CT acquisitions.

We have observed from our results (Fig. 6) that for selected patients these 3 steps alone were not able to obtain in general small errors in predicting MBF. However, for the patients with no ischemia we were able to precisely predict the tetra-colorimetric maps which often are enough for clinicians to make a diagnosis. Instead, for CAD patients and in general when considering the complete maps, the agreement significantly deteriorated.

A crucial role in the accurate prediction of MBF was demonstrated by the inclusion of step C4 that incorporated specific quantities extracted from the knowledge of the measured MBF_{CTP} . This still did not allow our computational prediction usable in current clinical practice. However, our results showed the ability of our tool to accurately predict MBF providing a fundamental and necessary first step in view of developing an effective predictive tool.

Several strategies could be investigated in future studies to improve steps C1-C3 and obtain the information needed by the model parameter circumventing step C4 and thus stress-CTP acquisition. For example, an IVN fitted with anatomical data [22] or machine learning techniques could be very useful for this purpose. In this way, the computational model will depend only on cCTA images and could be used in a predictive way to obtain MBF under stress avoiding the stress protocol.

Notice that this is not a statistical study, rather a computational one. This means that we built an a priori model based on the physical principles and not an a posteriori model based on data and measurements as required by statistics. For such a reason, our sample could not be considered too limited and it proved the validity of our model. We also notice that the computational time needed to obtain the

estimated MBF is about 12/15 hours per patient. This should not affect the clinical applicability of our method since it is not needed a real time answer.

The potential impact of this computational technique in the clinical assessment of patients with suspected CAD is of great interest. First, we notice that virtual scenarios with different perfusion conditions (different from the real one) could be simulated for a patient to understand the range of variability of her/his clinical answer. Moreover, the unique ability of cCTA to detect atherosclerosis non-invasively not only is fundamental for a mere diagnostic purpose but represents a key aspect in determining patient prognosis, as a prompt recognition of atherosclerotic plaques and subsequent appropriate medical management leads to significant reduction in major cardiovascular events [23]. For this reason, national and international societies decided to strengthen the indication to cCTA in the diagnostic work-up of patients with stable chest pain [24,25]. Interestingly, these guidelines recommended investigating further with functional imaging if the cCTA result is not diagnostic or atherosclerosis of uncertain degree is detected. Unfortunately, this chance is quite common, due to extensive calcific atherosclerotic burden often detected in patients with high likelihood of CAD [26]. Complementary assessment with myocardial ischaemia detection thus represents a mandatory step in the management of many patients with CAD. The possibility to get both anatomical and functional data with the same diagnostic test represents the most appealing strategy. Currently, CT is the only diagnostic technique capable to fulfil both needs: atherosclerotic detection with cCTA and functional assessment with either FFR_{CT} or Stress-CTP. Both combined approaches, cCTA+ FFR_{CT} and cCTA+Stress-CTP, have been shown to be very accurate in detecting functionally relevant coronary stenosis [5,27], with the advantage of FFR_{CT} analysis over Stress-CTP to be obtained without further radiation exposure and contrast administration [6]. Indeed, it is necessary to perform dynamic stress CTP acquisition after cCTA in order to obtain MBF estimation under stress conditions with a subsequent relevant increase of overall effective dose (MBF estimation can vary between 5 to 9 mSv according to different technology available). For this reason, the implementation of a computational method able to derive MBF estimation from a cCTA dataset can remarkably reduce the overall radiation exposure. Computational approaches, as proved by HeartFlow, are accurate, reproducible, cost-effective [28], safe in minimizing biological exposure to radiation dose and iodinated contrast, effective in correctly stratifying patient prognosis, and safe in avoiding unnecessary invasive coronary angiography [29]. However, this approach is limited to the assessment of the epicardial component of the coronary

vascular bed. Instead, the computational model provided in this study, being focused on the MBF estimation rather than the FFR, could provide crucial insight about another element of the coronary physiology, i.e. the microvascular compartment.

Limitations

Several are the limitations of the work. First, the consistency test has been performed by using the knowledge of CT-stress MBF to calibrate the parameters. This is of course not directly usable in the clinical practice. However, we believe that this test was mandatory in order to understand the reliability and future application of our method.

A second limitation relies in step C3 of the calibration process. In this work we have used the same factor (5), tuned in a heuristic way, for all patients to increase the conductances at the septum. More patient specific adjustments will be needed for future studies based on a deeper knowledge of why at the septum there was a systematic underestimation of blood flow maps.

Also, further investigations on the impact of a stenotic coronary tract on the perfusion will be needed to improve the computational model. In particular, the 3D fluid-dynamics problem accounts for the presence of a stenosis since the reconstructed geometry of the stenotic tract is used for the computational study. Besides this, it should be also investigated how conductances in the multi-compartment model could be modified by the presence of a proximal stenosis.

Table 1 Characteristics of the study population

Patient ID	Age (yrs)	Gender	BMI (kg/m²)	Risk factors	Symptoms	CAD-RADS
P1	55	M	30	1-5	TA	1
P2	64	F	23	3-5	TA	2
P3	72	M	19	-	TA	4B
P4	53	M	26	2-3-5	TA	4A
P5	69	M	26	1-2-3-5	TA	4B
P6	61	M	25	2-4-5	TA	3
P7	71	M	28	1-2-3-4-5	TA	4A
P8	61	M	30	1	TA	4A
P9	76	M	23	2-5	AA	5

BMI = body mass index; Risk factors: 1 = hypertension; 2 = smoker; 3 = hyperlipidemia; 4 = diabetes; 5 = family history of coronary artery disease; TA= typical angina; AA = atypical angina; CAD-RADS = Coronary Artery Disease Reporting and Data System

Table 2 Characteristics of cCTA scan protocols and stress parameters of the study population

Patient ID	Rest cCTA scan protocol					Stress-CTP scan protocol				
	HR before scanning (bpm)	β -blocker dosage (mg)	HR during scanning (bpm)	DLP (mGy-cm)	ED (mS v)	HR during scanning (bpm)	DLP (mGy-cm)	ED (mS v)	MBF _{avg} (ml/min/100ml)	% Perfused volume (left/right)
P1	70	10	63	195.97	2.74	85	432.00	8.79	334.25	66.1/33.9
P2	56	0	55	56.05	0.78	94	379.17	6.09	314.94	55.9/44.1
P3	58	0	57	177.13	2.48	69	396.86	8.04	246.75	72.3/27.7
P4	100	15	70	165.39	2.32	75	376.70	7.59	281.38	73.7/26.3
P5	67	5	57	213.84	2.99	74	380.08	8.31	172.51	68.8/31.2
P6	59	0	55	64.40	0.90	68	393.22	6.41	165.95	79.3/20.7
P7	50	0	42	288.47	4.04	64	401.71	9.66	121.86	67.7/32.3
P8	78	0	81	252.40	3.53	97	347.99	8.41	151.74	67.2/32.8
P9	60	0	59	192.64	2.70	61	422.81	8.62	122.93	62.7/37.3

HR = heart rate; cCTA = coronary computed tomography angiography; stress-CTP = stress myocardial computed tomography perfusion; DLP = Dose length product; ED = Effective Dose; MBF_{avg} = average myocardial blood flow from stress-CTP

Table 3. Number of perfusion regions and mean error in the estimation of myocardial blood flow.

Patient ID	Number of perfusion regions	Err_{mean} [%]
P1	19	1.07 ± 1.34
P2	15	1.79 ± 1.30
P3	21	1.05 ± 0.62
P4	27	0.98 ± 0.70
P5	25	1.27 ± 0.72
P6	29	1.65 ± 1.30
P7	29	2.78 ± 0.15
P8	25	3.54 ± 2.04
P9	46	2.32 ± 1.31

Err_{mean} values ± SD. Err_{mean} = weighted mean among the perfusion regions of discrepancies between measured and computational myocardial blood flow.

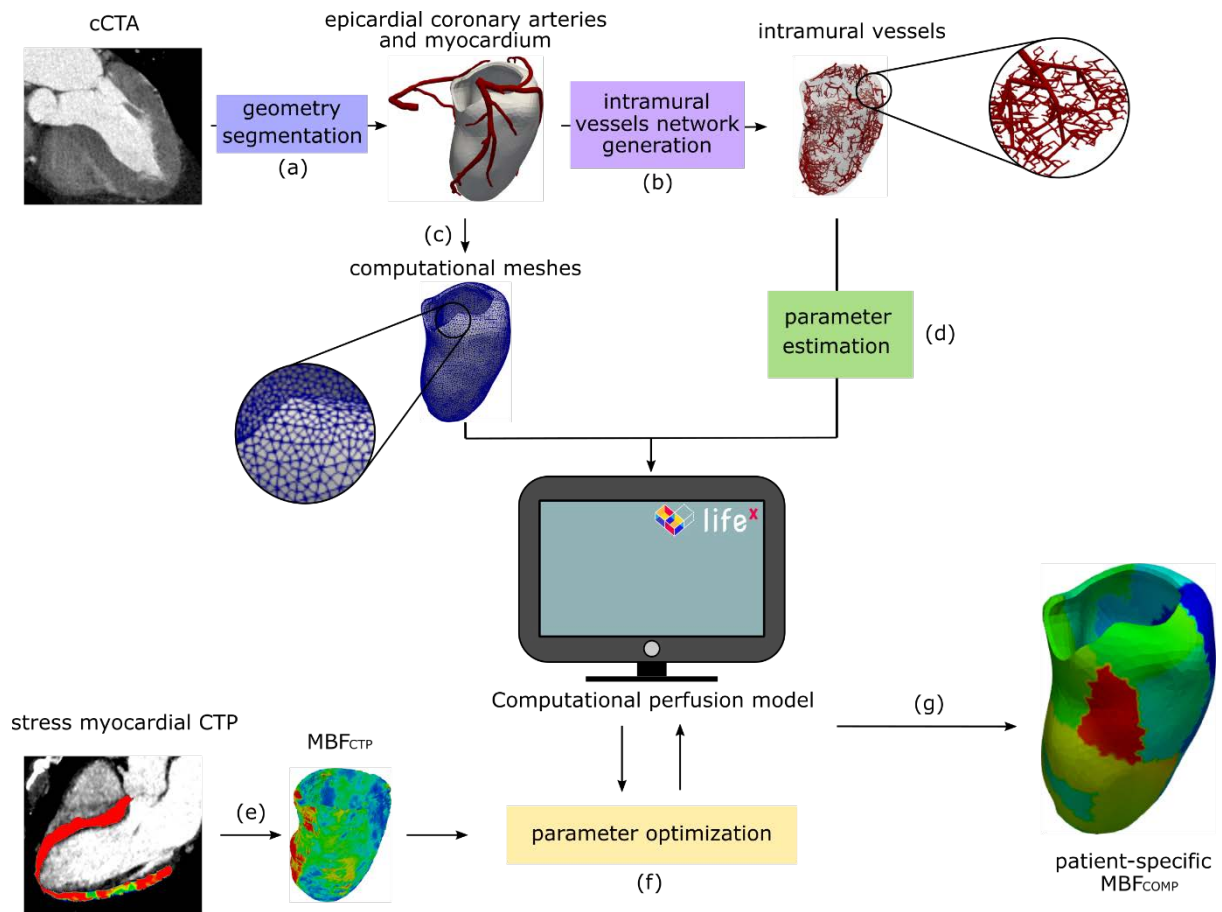


Figure 1. Generation of computational myocardial perfusion. a) Geometry reconstruction from cCTA; b) generation of the intramural vascular network; c) generation of the computational meshes; d) estimation of parameters - steps C1-C3; e) measurement of MBF_{CTP} map from stress CTP; f) optimization of parameters guided by MBF_{CTP} - step C4; g) computation of MBF_{COMP}. CT = computed tomography; cCTA = coronary computed tomography angiography; CTP = computed tomography perfusion; MBF_{COMP} = computational myocardial blood flow; MBF_{CTP} = measured myocardial blood flow.

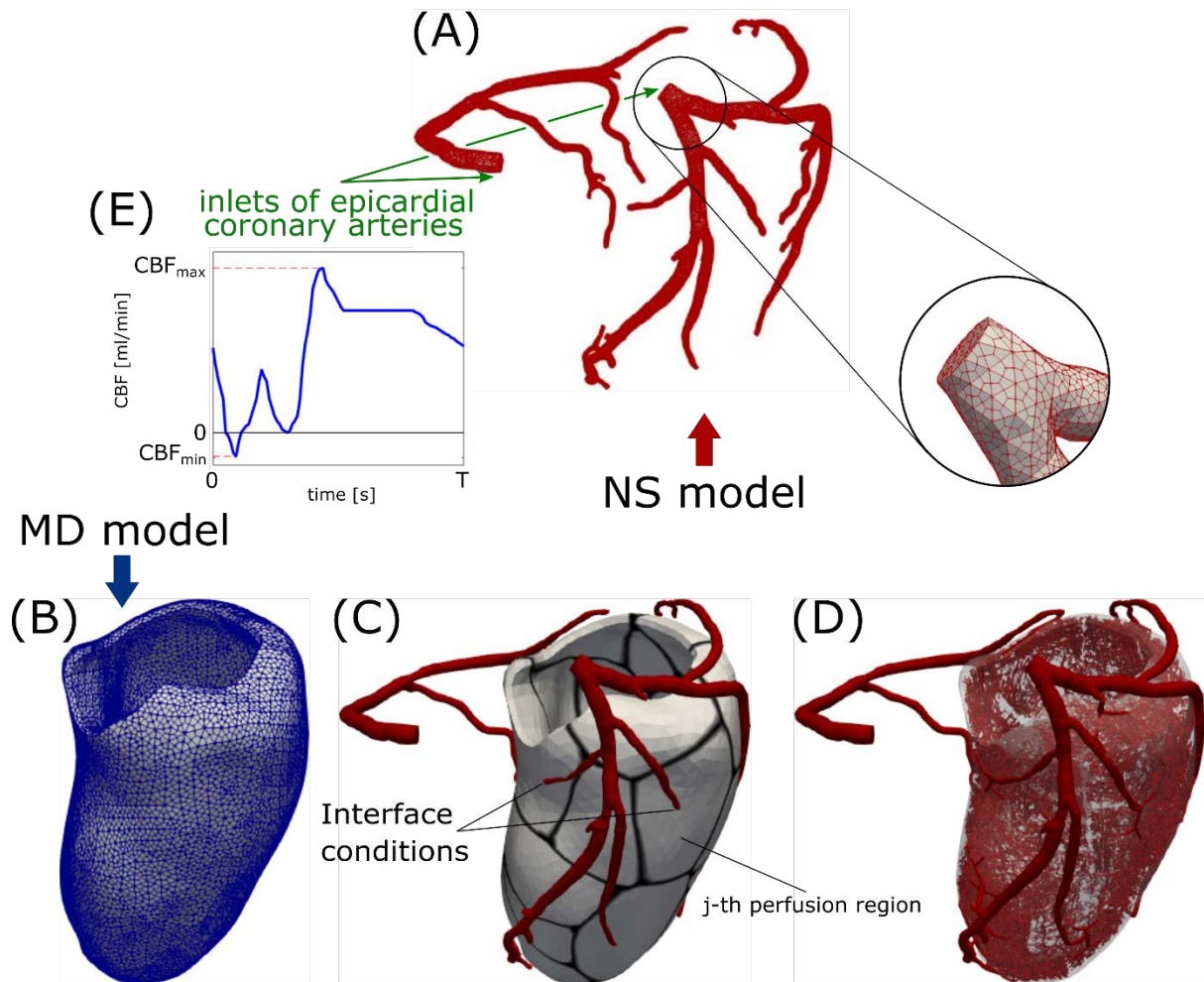


Figure 2. Example of geometry reconstruction in patient P4. (A) Mesh of epicardial coronary arteries; (B) mesh of the myocardium; (C) epicardial coronary arteries with perfusion regions; (D) epicardial coronary arteries with the surrogate intramural vascular network; (E) inlet coronary blood flow profile (blue). CBF = coronary blood flow; T = heartbeat period.

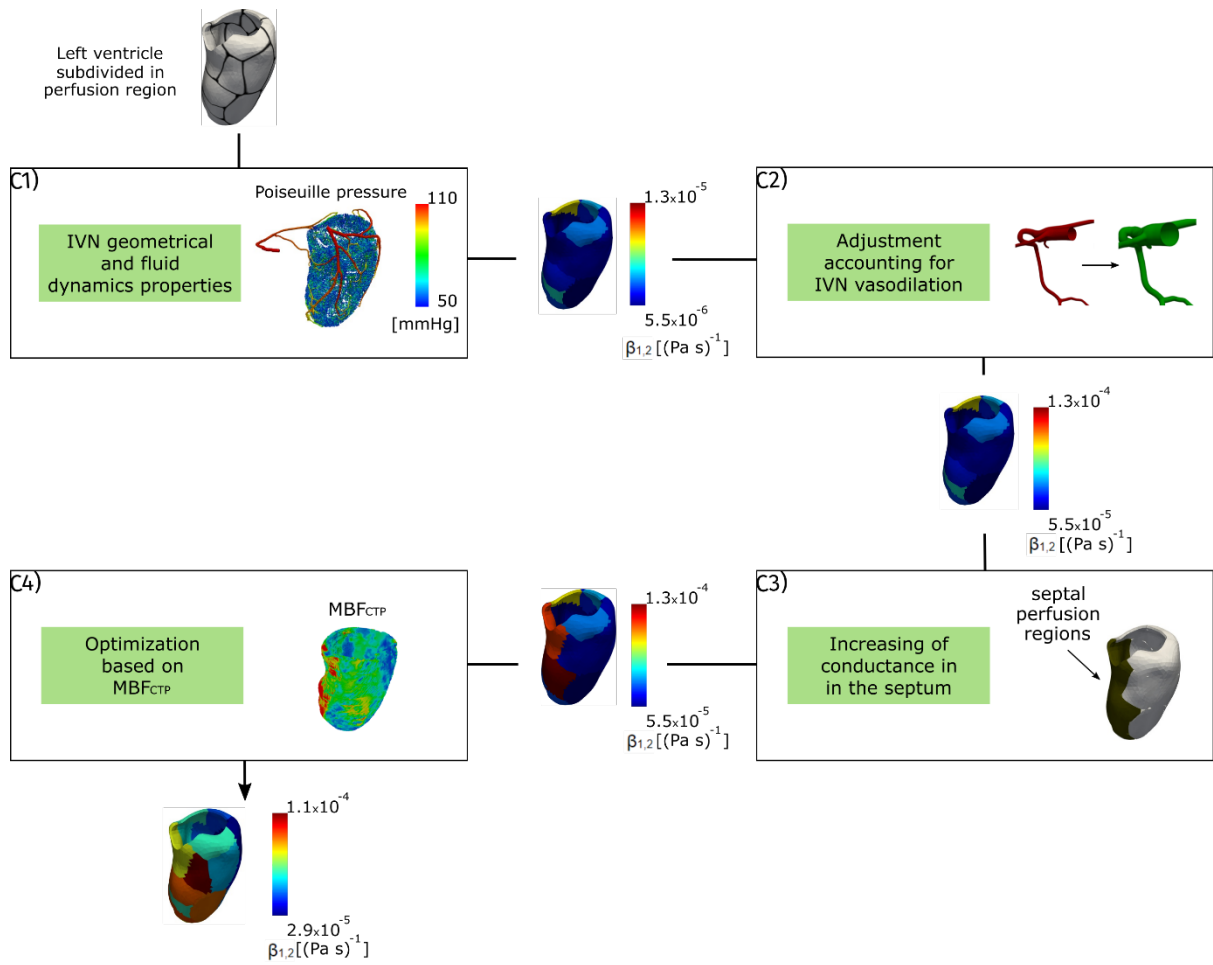


Figure. 3 Schematic representation of the calibration procedure.

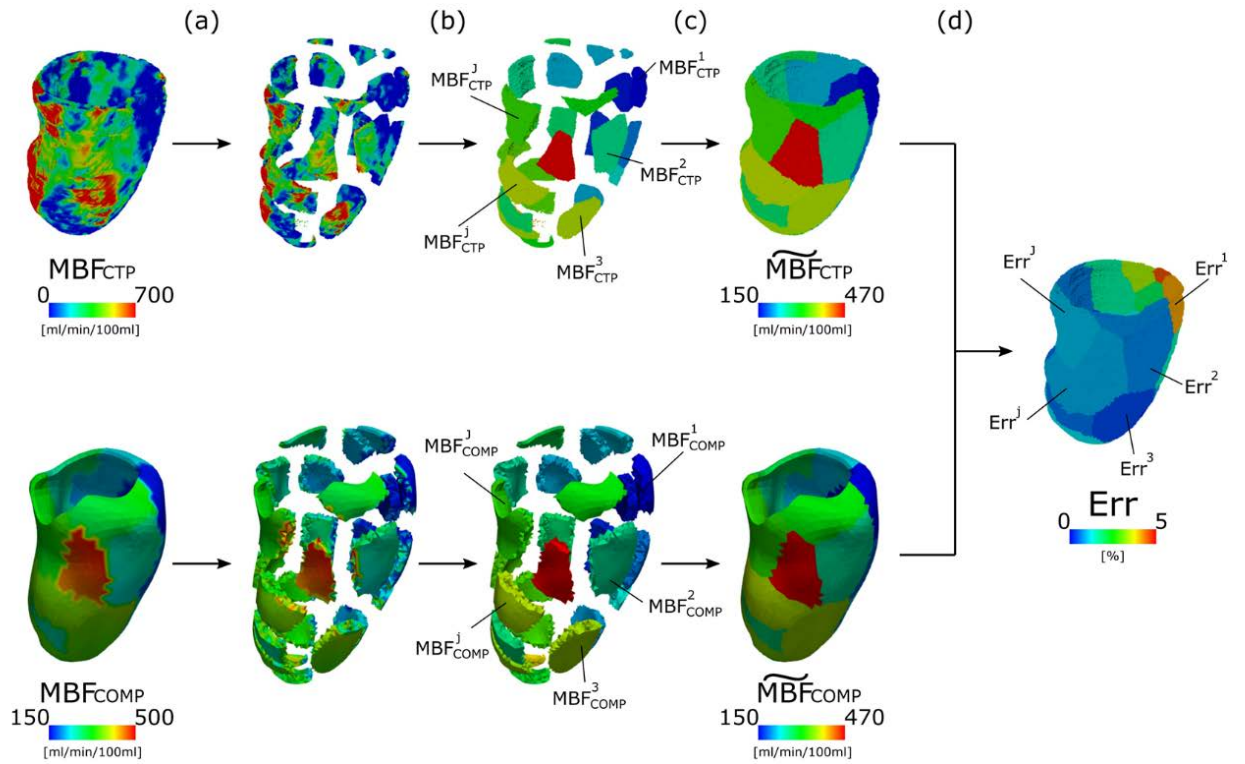


Figure 4. Computation of the relative error between MBF_{CTP} (top) and MBF_{COMP} (bottom): (a) subdivision in perfusion regions; (b) computation of the average-in-space MBF for each perfusion region; (c) collection of all MBF_{CTP}^i and MBF_{COMP}^i in a unique map (\widetilde{MBF}_{CTP} and \widetilde{MBF}_{COMP}); (d) computation of the relative error. Err = relative error between \widetilde{MBF}_{CTP} and \widetilde{MBF}_{COMP} . \widetilde{MBF}_{COMP} = averages in space of measured perfusion maps; \widetilde{MBF}_{CTP} = averages in space of computational perfusion maps.

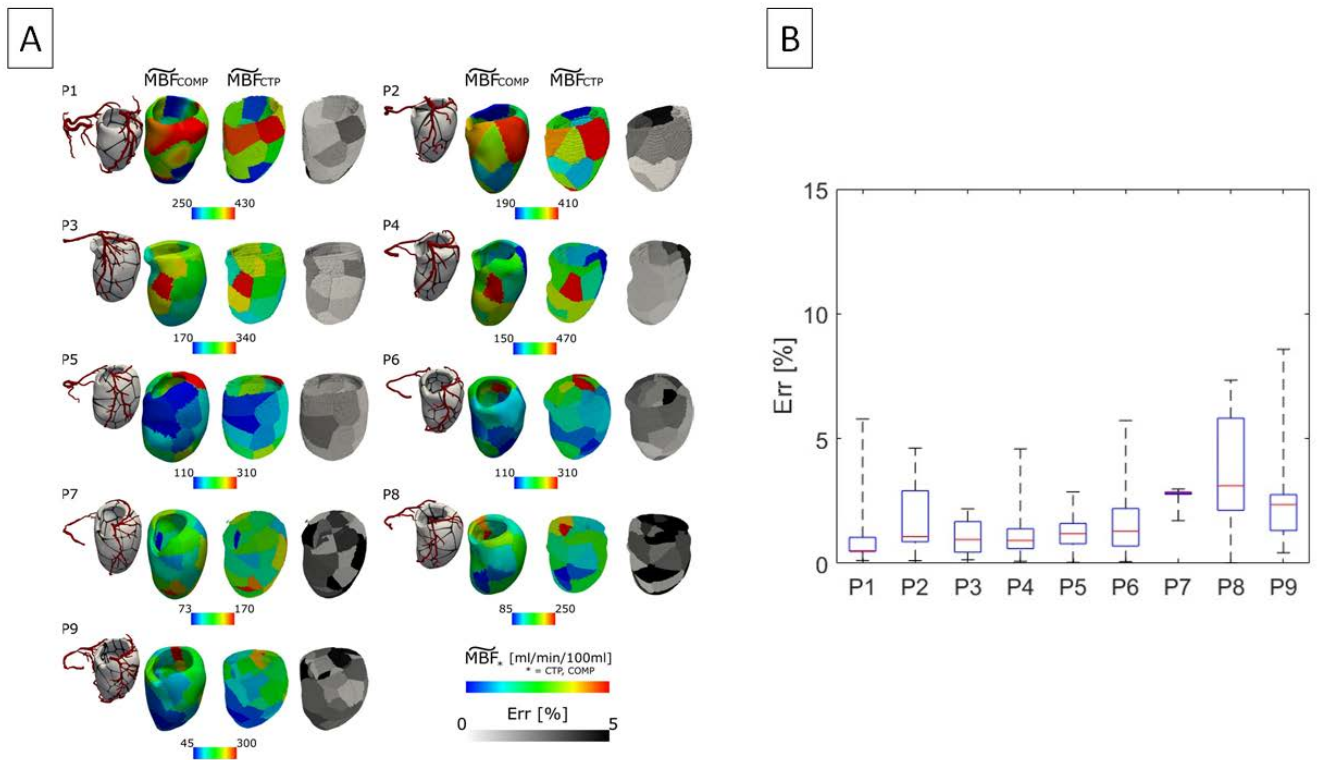


Figure 5. Panel A. From left to right: reconstructed epicardial coronaries and myocardium with perfusion regions; \overline{MBF}_{COMP} ; \overline{MBF}_{CTP} ; Err. **Panel B.** Boxplots of Err for each patient. Err = relative error in all the perfusion regions. Abbreviations as in Fig. 4.

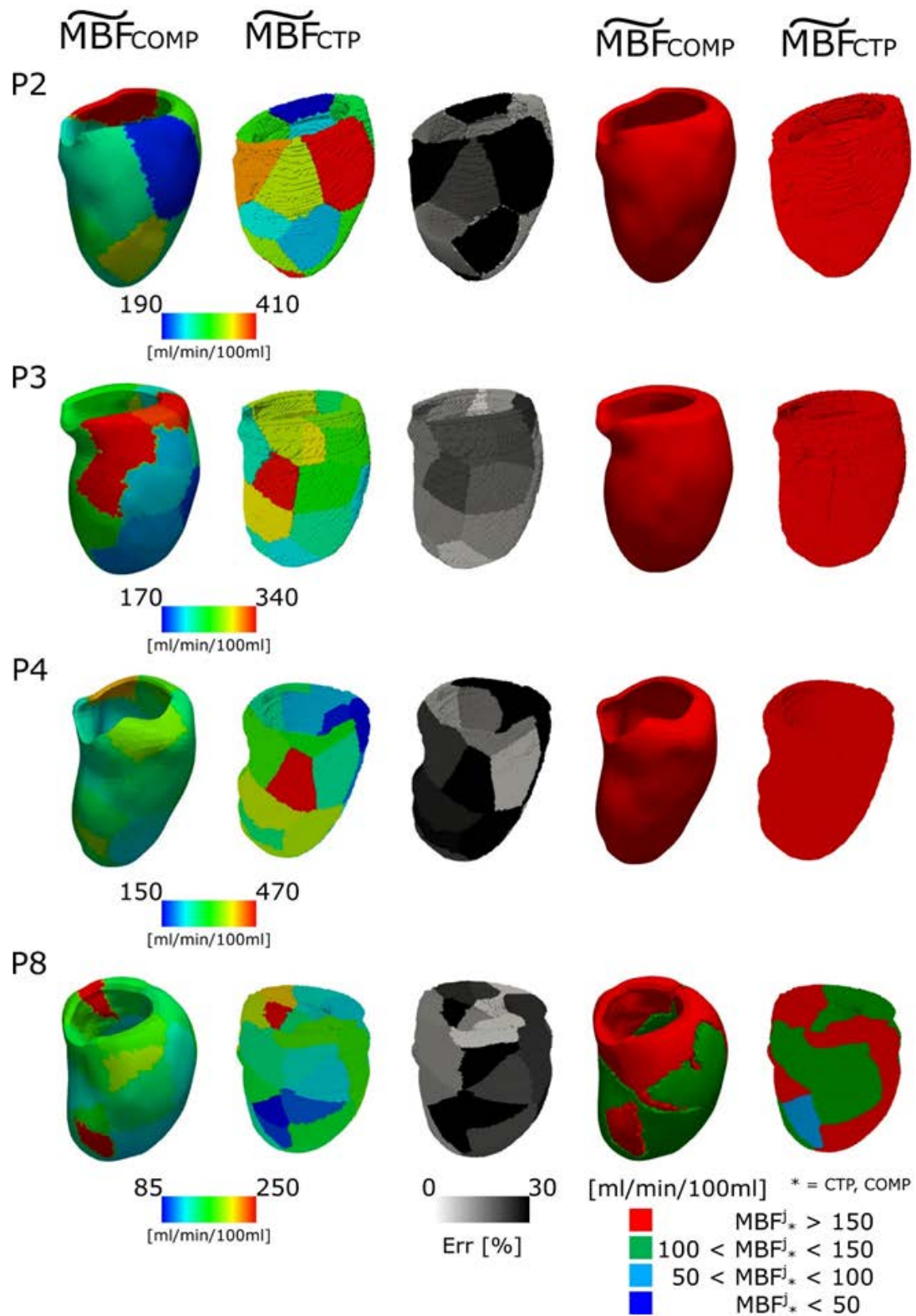


Figure 6. Left: \overline{MBF}_{COMP} and \overline{MBF}_{CTP} ; Middle: Percentage error Err; Right: \overline{MBF}_{COMP} and \overline{MBF}_{CTP} in the tetra-colorimetric maps. 4 selected cases (P2,P3,P4,P8). Abbreviations as in Fig. 4.

Author contributions

Conceptualization: Simone Di Gregorio, Christian Vergara, Gianluca Pontone.

Methodology: Simone Di Gregorio, Christian Vergara, Paolo Zunino, Giovanni Montino Pelagi.

Formal analysis and investigation: Simone Di Gregorio, Giovanni Montino Pelagi.

Writing - original draft preparation: Simone Di Gregorio, Christian Vergara.

Writing - review and editing: Simone Di Gregorio, Christian Vergara, Andrea Baggiano, Marco Guglielmo, Laura Fusini, Giuseppe Muscogiuri, Alexia Rossi, Mark G Rabbat, Paolo Zunino, Alfio Quarteroni, Gianluca Pontone

Supervision: Gianluca Pontone, Alfio Quarteroni, Christian Vergara.

Funding: No funding was received for conducting this study.

DECLARATIONS

Conflict of interest: Pontone G. declared institutional research grant and/or honorarium as speaker from General Electric, Bracco, Heartflow.

Ethical Approval: Ethical Review Board approval was obtained (R250/15-CCM 262). All procedures performed in studies involving human participants were in accordance with the ethical standards of the institutional and/or national research committee and with the 1964 Helsinki declaration and its later amendments or comparable ethical standards

Informed Consent: Written informed consent was obtained from all subjects (patients) in this study

REFERENCES

1. Pontone G, Andreini D, Guaricci AI, Baggiano A, Fazzari F, Guglielmo M, et al. Incremental Diagnostic Value of Stress Computed Tomography Myocardial Perfusion With Whole-Heart Coverage CT Scanner in Intermediate- to High-Risk Symptomatic Patients Suspected of Coronary Artery Disease. *JACC Cardiovasc Imaging* 2019;12:338–49. doi: 10.1016/j.jcmg.2017.10.025
2. Pontone G, Andreini D, Guaricci AI, Guglielmo M, Baggiano A, Muscogiuri G, et al. Quantitative vs. qualitative evaluation of static stress computed tomography perfusion to detect haemodynamically significant coronary artery disease. *Eur Heart J Cardiovasc Imaging* 2018;19:1244–52. doi: 10.1093/ehjci/je111
3. Pontone G, Baggiano A, Andreini D, Guaricci AI, Guglielmo M, Muscogiuri G, et al. Diagnostic accuracy of simultaneous evaluation of coronary arteries and myocardial perfusion with single stress cardiac computed tomography acquisition compared to invasive coronary angiography plus invasive fractional flow reserve. *Int J Cardiol* 2018;273:263–8. doi: 10.1016/j.ijcard.2018.09.065
4. Pontone G, Baggiano A, Andreini D, Guaricci AI, Guglielmo M, Muscogiuri G, et al. Stress Computed Tomography Perfusion Versus Fractional Flow Reserve CT Derived in Suspected Coronary Artery Disease: The PERFECTION Study. *JACC Cardiovasc Imaging* 2019;12:1487–97. doi: 10.1016/j.jcmg.2018.08.023
5. Pontone G, Baggiano A, Andreini D, Guaricci AI, Guglielmo M, Muscogiuri G, et al. Dynamic Stress Computed Tomography Perfusion With a Whole-Heart Coverage Scanner in Addition to Coronary Computed Tomography Angiography and Fractional Flow Reserve Computed Tomography Derived. *JACC Cardiovasc Imaging* 2019;12:2460–71. doi: 10.1016/j.jcmg.2019.02.015
6. Baggiano A, Fusini L, Del Torto A, Vivona P, Guglielmo M, Muscogiuri G, et al. Sequential Strategy Including FFRCT Plus Stress-CTP Impacts on Management of Patients with Stable Chest Pain: The Stress-CTP RIPCORDER Study. *J Clin Med* 2020;9:2147. doi: 10.3390/jcm9072147
7. Alves JR, de Queiroz RAB, Bär M, dos Santos RW. Simulation of the Perfusion of Contrast Agent Used in Cardiac Magnetic Resonance: A Step Toward Non-invasive Cardiac Perfusion Quantification. *Front Physiol* 2019;10:177. doi: 10.3389/fphys.2019.00177
8. Chapelle D, Gerbeau J-F, Sainte-Marie J, Vignon-Clementel IE. A poroelastic model valid in large strains with applications to perfusion in cardiac modeling. *Computational Mechanics* 2009;46(1):91–101. doi:10.1007/s00466-009-0452-x

9. Di Gregorio S, Fedele M, Pontone G, Corno AF, Zunino P, Vergara C, et al. A computational model applied to myocardial perfusion in the human heart: from large coronaries to microvasculature. *J Comput Phys* 2021;424:109836. doi: 10.1016/j.jcp.2020.109836
10. Lee J, Cookson A, Chabiniok R, Rivolo S, Hyde E, Sinclair M, et al. Multiscale Modelling of Cardiac Perfusion. In: Quarteroni A (eds) *Modeling the Heart and the Circulatory System*. MS&A, 2015;14:51–96.
11. Namani R, Lee LC, Lanir Y, Kaimovitz B, Shavik SM, Kassab GS. Effects of myocardial function and systemic circulation on regional coronary perfusion. *J Appl Physiol* 2020;128:1106–22. doi: 10.1152/jappphysiol.00450.2019
12. Papamanolis L, Kim HJ, Jaquet C, Sinclair M, Schaap M, Danad I, et al. Myocardial Perfusion Simulation for Coronary Artery Disease: A Coupled Patient-Specific Multiscale Model. *Ann Biomed Eng* 2021;49:1432-47. doi: 10.1007/s10439-020-02681-z
13. So A, Hsieh J, Li YY, Hadway J, Kong HF, Lee TY. Quantitative myocardial perfusion measurement using CT Perfusion: a validation study in a porcine model of reperfused acute myocardial infarction. *Int J Cardiovasc Imaging* 2012;28:1237–48. doi: 10.1007/s10554-011-9927-x
14. Antiga L, Piccinelli M, Botti L, Ene-Iordache B, Remuzzi A, Steinman DA. An image-based modeling framework for patient-specific computational hemodynamics. *Med Biol Eng Comput* 2008;46:1097-112. doi: 10.1007/s11517-008-0420-1
15. Fedele M. and Quarteroni A. Polygonal surface processing and mesh generation tools for the numerical simulation of the cardiac function. *Int J Numer Meth Biomed Engng* 2021;e3435. doi: 10.1002/cnm.3435
16. Michler C, Cookson AN, Chabiniok R, Hyde E, Lee J, Sinclair M, et al. A computationally efficient framework for the simulation of cardiac perfusion using a multi-compartment Darcy porous-media flow model. *Int J Numer Method Biomed Eng* 2013;29:217-32. doi: 10.1002/cnm.2520
17. Hyde ER, Cookson AN, Lee J, Michler C, Goyal A, Sochi T, et al. Multi-Scale Parameterisation of a Myocardial Perfusion Model Using Whole-Organ Arterial Networks. *Ann Biomed Eng* 2014;42:797-811. doi: 10.1007/s10439-013-0951-y
18. Ponzini R, Vergara C, Redaelli A, Veneziani A. Reliable CFD-based estimation of flow rate in haemodynamics measures. *Ultrasound Med Biol* 2006;32:1545–55. doi: 10.1016/j.ultrasmedbio.2006.05.022

19. Tezduyar T, Sathe S. Stabilization parameters in SUPG and PSPG formulations. *J Comput Appl Mech* 2003;4:71-88.
20. Arndt D, Bangerth W, Clevenger TC, Davydov V, Fehling M, Garcia-Sanchez D, et al. The deal.II library, Version 9.1. *J Numer Math* 2019;27:203–13. doi: 10.1515/jnma-2019-0064
21. Zhang C, A Rogers P, Merkus D, Muller-Delp JM, Tiefenbacher CP, Potter B, et al. Regulation of Coronary Microvascular Resistance in Health and Disease. In: Tuma RF, Durán WN, Ley K (eds) *Microcirculation* 2008;521–49.
22. Kaimovitz B, Lanir Y, Kassab GS. Large-scale 3-D geometric reconstruction of the porcine coronary arterial vasculature based on detailed anatomical data. *Ann Biomed Eng* 2005;33:1517-35. doi: 10.1007/s10439-005-7544-3
23. SCOT-HEART Investigators, Newby DE, Adamson PD, Berry C, Boon NA, Dweck MR, et al. Coronary CT Angiography and 5-Year Risk of Myocardial Infarction. *N Engl J Med* 2018;379:924-33. doi: 10.1056/NEJMoa1805971
24. Timmis A, Roobottom CA. National Institute for Health and Care Excellence updates the stable chest pain guideline with radical changes to the diagnostic paradigm. *Heart* 2017;103:982-6. doi: 10.1136/heartjnl-2015-308341
25. Knuuti J, Wijns W, Saraste A, Capodanno D, Barbato E, Funck-Brentano C, et al. 2019 ESC Guidelines for the diagnosis and management of chronic coronary syndromes. *Eur Heart J* 2020;41:407–77.
26. Pontone G, Bertella E, Mushtaq S, Loguercio M, Cortinovis S, Baggiano A, et al. Coronary Artery Disease: Diagnostic Accuracy of CT Coronary Angiography- - A Comparison of High and Standard Spatial Resolution Scanning. *Radiology* 2014;271:688–94. doi: 10.1148/radiol.13130909
27. Nørgaard BL, Leipsic J, Gaur S, Seneviratne S, Ko BS, Ito H, et al. Diagnostic Performance of Noninvasive Fractional Flow Reserve Derived From Coronary Computed Tomography Angiography in Suspected Coronary Artery Disease. *J Am Coll Cardiol* 2014;63:1145-55. doi: 10.1016/j.jacc.2013.11.043
28. Hlatky MA, De Bruyne B, Pontone G, Patel M, Norgaard BL, Byrne RA, et al. Quality-of-life and economic outcomes of assessing fractional flow reserve with computed tomography angiography: PLATFORM. *J Am Coll Cardiol* 2015, 66:2315-23. doi: 10.1016/j.jacc.2015.09.051

29. Fairbairn TA, Nieman K, Akasaka T, Norgaard BL, Berman DS, Raff G, et al. Real-world clinical utility and impact on clinical decision-making of coronary computed tomography angiography-derived fractional flow reserve: lessons from the ADVANCE Registry. *Eur Heart J* 2018,39:3701-11. doi: 10.1093/eurheartj/ehy530

MOX Technical Reports, last issues

Dipartimento di Matematica
Politecnico di Milano, Via Bonardi 9 - 20133 Milano (Italy)

- 93/2021** Parolini, N.; Dede', L.; Ardenghi, G.; Quarteroni, A.
Modelling the COVID-19 epidemic and the vaccination campaign in Italy by the SUIHTER model
- 92/2021** Antonietti, P.F.; Manzini, G.; Scacchi, S.; Verani, M.
On arbitrarily regular conforming virtual element methods for elliptic partial differential equations
- 94/2021** Antonietti, P.F.; Berrone, S.; Busetto, M.; Verani, M.
Agglomeration-based geometric multigrid schemes for the Virtual Element Method
- 86/2021** Possenti, L.; Cicchetti, A.; Rosati, R.; Cerroni, D.; Costantino, M.L.; Rancati, T.; Zunino, P.
A Mesoscale Computational Model for Microvascular Oxygen Transfer
- 87/2021** Both, J.W.; Barnafi, N.A.; Radu, F.A.; Zunino, P.; Quarteroni, A.
Iterative splitting schemes for a soft material poromechanics model
- 88/2021** Kuchta, M.; Laurino, F.; Mardal, K.A.; Zunino, P.
Analysis and approximation of mixed-dimensional PDEs on 3D-1D domains coupled with Lagrange multipliers
- 90/2021** Hernandez, V.M.; Paolucci, R.; Mazzieri, I.
3D numerical modeling of ground motion in the Valley of Mexico: a case study from the Mw3.2 earthquake of July 17, 2019
- 85/2021** Cavinato, L., Gozzi, N., Sollini, M., Carlo-Stella, C., Chiti, A., & Ieva, F.
Recurrence-specific supervised graph clustering for subtyping Hodgkin Lymphoma radiomic phenotypes
- 91/2021** Arnone, E.; Sangalli, L.M.; Vicini, A.
Smoothing spatio-temporal data with complex missing data patterns
- 84/2021** Torti, A.; Galvani, M.; Urbano, V.; Arena, M.; Azzone, G.; Secchi, P.; Vantini, S.
Analysing transportation system reliability: the case study of the metro system of Milan